

Lend me an Ear: Speech Enhancement Using a Robotic Arm with a Microphone Array

Zachary Turcotte and François Grondin

Abstract—Speech enhancement performance degrades significantly in noisy environments, limiting the deployment of speech-controlled technologies in industrial settings, such as manufacturing plants. Existing speech enhancement solutions primarily rely on advanced digital signal processing techniques, deep learning methods, or complex software optimization techniques. This paper introduces a novel enhancement strategy that incorporates a physical optimization stage by dynamically modifying the geometry of a microphone array to adapt to changing acoustic conditions. A sixteen-microphone array is mounted on a robotic arm manipulator with seven degrees of freedom, with microphones divided into four groups of four, including one group positioned near the end-effector. The system reconfigures the array by adjusting the manipulator joint angles to place the end-effector microphones closer to the target speaker, thereby improving the reference signal quality. This proposed method integrates sound source localization techniques, computer vision, inverse kinematics, minimum variance distortionless response beamformer and time-frequency masking using a deep neural network. Experimental results demonstrate that this approach outperforms other traditional recording configurations, achieving higher scale-invariant signal-to-distortion ratio and lower word error rate across multiple input signal-to-noise ratio conditions.

I. INTRODUCTION

The current labour shortage affects many manufacturing sectors in industrialized countries, and the integration of robots into the workforce has emerged as a potential solution. To ease this transition, worker-robot interaction must be intuitive, with speech-based instructions representing a natural and efficient communication modality [1], [2], [3]. Compared with alternative control interfaces, such as a touchscreens or keyboard-based inputs, speech has been shown to be the most efficient human-robot interaction method [2], [4]. For instance, [4] demonstrated successful speech-based control of an industrial manipulator. When combined with a vision module and a large language model-driven agent, the system achieved a high success rate in understanding instructions and executing them. However, reliable operation of such systems requires clean speech signals. In industrial environments, microphones capture both speech and background noise, which significantly degrades the performance of automatic speech recognition (ASR) systems.

Speech enhancement (SE) methods can generally be categorized into single-channel and multichannel approaches.

This work was supported by the Natural Sciences and Engineering Research Council of Canada and the Canada Foundation of Innovation. Zachary Turcotte and François Grondin are with Department of Electrical and Computer Engineering, Université de Sherbrooke, Québec, Canada. zachary.turcotte@usherbrooke.ca, francois.grondin2@usherbrooke.ca

Multichannel techniques are especially advantageous because they can leverage spatial information obtained from multiple microphones. By exploiting spatial cues, these methods typically achieve improved noise reduction and lower signal distortion, which in turn enhances the reliability of ASR systems.

Most multichannel SE approaches rely on beamforming techniques, and modern methods can be classified into three main categories: 1) Hybrid approaches use a Deep Neural Network (DNN) to estimate statistical properties of the noisy signal, such as an ideal ratio mask (IRM), which is then used to estimate the speech and noise covariance matrices (SCMs). The estimated SCMs are subsequently employed to compute the coefficients of a spatial filter, such as the Minimum Variance Distortionless Response (MVDR) or Generalized Eigenvalue Decomposition (GEV) beamformer [5], [6]; 2) A DNN directly predicts the beamforming filter coefficients from the noisy input signal [7], [8]. The network learns a mapping between the observed noisy signals and the optimal spatial filter weights, with the goal of learning beamformers that outperform analytically derived solutions; 3) End-to-end approach map raw audio signals or noisy short-time Fourier transform (STFT) features to either clean signal or the predicted text outputs [9] [10]. The network learns to transform noisy inputs into clean outputs without explicitly modeling intermediate beamforming steps. These models are often trained jointly with language models, as ASR is typically the final stage of the processing pipeline.

However, the performance of these enhancement algorithms deteriorates with the presence of strong background noise, making it challenging to deploy voice-controlled technology in a manufacturing environments where noise is pervasive and continuous. Most microphone arrays used in robotic applications have a fixed geometry [11], [12]. While arrays mounted on mobile robots change their absolute position, the relative placement of the microphones remains constant. The geometry of a microphone array plays a critical role in beamforming performance [13], [14], [15], [16], as it influences the spatial filtering properties of the array. In this work, we propose to mount microphones on an industrial manipulator and to leverage its articulated joints to dynamically reconfigure the microphone array geometry in real time. This approach enables the system to adapt its spatial configuration to the current acoustic conditions, potentially improving speech enhancement performance in challenging industrial environments.

The paper is organized as follows. Section II presents the entire enhancement pipeline, from SSL to speech enhance-

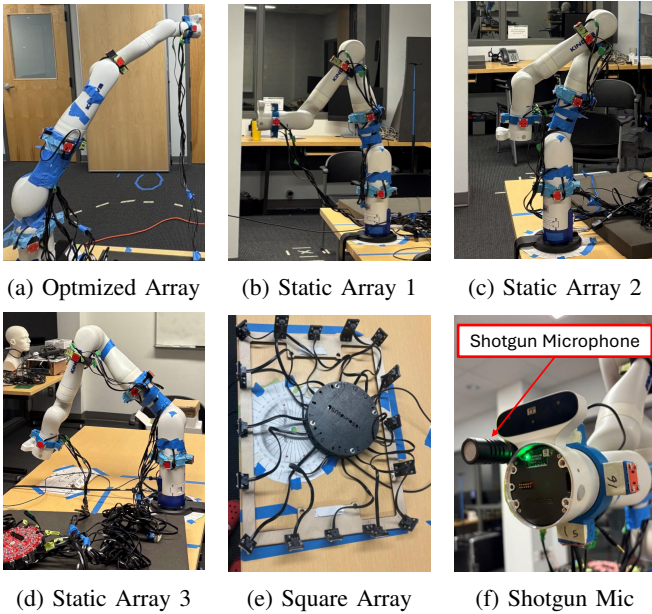


Fig. 1: All recording devices used during experiments

ment (SE). Section III assess the performance of the system. Finally, section IV concludes this paper and discusses future work.

II. PROPOSED METHOD

A. Hardware setup

The system consists of a Kinova Gen3 robotic arm with seven degrees of freedom and equipped with 16 omnidirectional microphones. These microphones are separated into four sub-arrays positioned on different joints of the robotic arm, including one sub-array located near the end-effector. The microphones are connected to the 16SoundsUSB sound card¹. Figure 2 illustrates the precise placement of the sub-arrays and the complete experimental setup. The Gen3 is also equipped with an Omnivision 5640 RGB camera and a Intel RealSense Depth Module D410.

B. Enhancement pipeline

The SE pipeline is divided into five submodules, as illustrated in Fig. 3. The first module consists of a DNN that predicts ideal ratio masks (IRM). The second part is a SSL module that estimates the approximate direction of arrival (DoA) of the target. Due to the presence of robotic arm components between the microphones and the array's wide geometry, the free-field and far-field assumptions are violated, resulting in only approximate DoA estimation. Furthermore, the microphone positions vary with the arm configuration, preventing the use of methods based on fixed acoustic transfer functions, such as head-related transfer functions (HRTF). To refine target localization, the system leverages the integrated RGB camera and depth sensor. After obtaining an approximate azimuth angle from the SSL module, the robotic arm rotates so that both cameras are oriented

¹<https://github.com/introlab/16SoundsUSB>

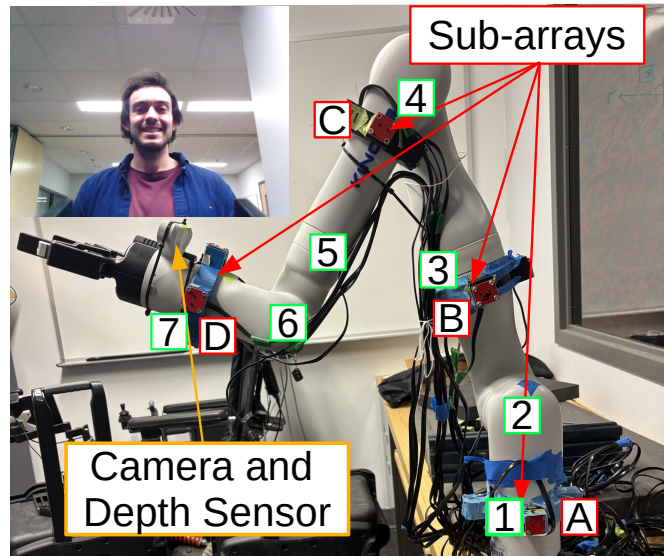


Fig. 2: Experimental setup. Red markers indicate the site where the sub-arrays are located on the robotic arm. Green markers indicate the joint number.

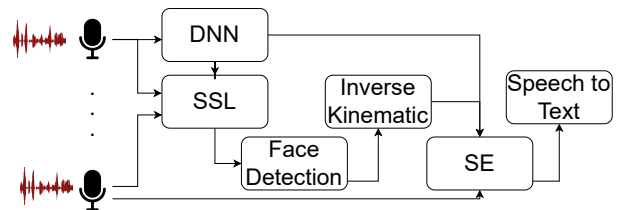


Fig. 3: Enhancement pipeline

toward the target. The third module uses the camera and depth sensor to localize the speaker in 3-d space. The fourth module consists of the inverse kinematic (IK) solver provided by Kinova. The IK module receives the speaker localization and computes the joint angles required for the arm to reach an optimal listening position. The robotic arm subsequently repositions itself into the optimized configuration, illustrated in Fig. 1a. The fifth module applies a MVDR beamformer combined with a DNN-based IRM estimator. This SE method is selected because it is inherently agnostic to the microphone array geometry.

C. Signal Model

The signal can be modeled in the time-frequency domain as $\mathbf{Y}(t, f) = \mathbf{X}(t, f) + \mathbf{B}(t, f)$, where $\mathbf{Y}(t, f) \in \mathbb{C}^{K \times 1}$ stands for the Short-Time-Fourier-Transform (STFT) of noisy recorded signal for $K \in \mathbb{N}$ microphones, $\mathbf{X}(t, f) \in \mathbb{C}^{K \times 1}$ for the STFT of the clean speech and $\mathbf{B}(t, f) \in \mathbb{C}^{K \times 1}$ for the STFT of the noise. Variables $t \in \{1, 2, \dots, T\}$ and $f \in \{0, 1, \dots, N/2\}$ stand for the frame time index for a total of T frames and the frequency bin with a N sample analysis window, respectively.

D. Ideal Ratio Masks estimation

For both SE and SSL modules, it is essential to separate the target speech component $X_k(t, f) \in \mathbb{C}$ and the

background noise component $B_k(t, f) \in \mathbb{C}$ from the noisy observation $Y_k(t, f) \in \mathbb{C}$ at each microphone k to achieve optimal performance. The IRM is an effective approach for performing this separation and is defined by:

$$M_k(t, f) = \min \left(\max \left(\frac{|X_k(t, f)|}{|X_k(t, f)| + |B_k(t, f)|}, 0 \right), 1 \right), \quad (1)$$

where $M_k(t, f) \in [0, 1]$ stands for the mask at frequency bin f , time frame t and microphone k . The operator $|\cdot|$ denotes the magnitude of a complex value. DNNs provide an effective way to estimate IRMs, and several network architectures have been proposed for this task. In this study, a recurrent neural network (RNN) is used due to its relatively simple architecture and good performance. The input of the DNN is $\log|Y(t, f)|$. The network begins with a batch normalization (BN) layer, followed by two bidirectional long short-term memory (BLSTM) layers with 1024 hidden units each. The final layer is a fully connected (FC) layer with 257 output units, similar to the architecture proposed in SteerNet [17]. The network is trained using single-channel recordings from the DNS Challenge dataset [18]. Reverberation is added using the SLR28 dataset, which contains both simulated and measured room impulse responses (RIRs) [19]. During operation, the DNN processes the noisy input from all 16 channels and predicts 16 different masks $\{M_1(t, f), M_2(t, f), \dots, M_{16}(t, f)\}$.

E. Sound Source Localization

The steered-response-power phase transform (SRP-PHAT) algorithm with spatially whitened noise estimates the DoA of the target speaker. The key difference from the conventional SRP-PHAT method lies in the use of the online Spatial Covariance Matrices (oSCMs) of both the noise ($\hat{\Phi}_B(t, f) \in \mathbb{C}^{K \times K}$) and speech ($\hat{\Phi}_X(t, f) \in \mathbb{C}^{K \times K}$) components:

$$\hat{\Phi}_{XX}(t, f) = (1 - \alpha)\hat{\Phi}_{XX}(t-1, f) + \alpha\hat{\mathbf{R}}_{XX}(t, f), \quad (2)$$

$$\hat{\Phi}_{BB}(t, f) = (1 - \alpha)\hat{\Phi}_{BB}(t-1, f) + \alpha\hat{\mathbf{R}}_{BB}(t, f), \quad (3)$$

where

$$\hat{\mathbf{R}}_{XX}(t, f) = \hat{M}(t, f)\mathbf{Y}(t, f)\mathbf{Y}(t, f)^H, \quad (4)$$

$$\hat{\mathbf{R}}_{BB}(t, f) = (1 - \hat{M}(t, f))\mathbf{Y}(t, f)\mathbf{Y}(t, f)^H, \quad (5)$$

and $\alpha \in [0, 1]$ is the adaptation rate. The global mask $\hat{M}(t, f) \in \mathbb{R}$ is obtained as follows:

$$\hat{M}(t, f) = \max(\{M_1(t, f), M_2(t, f), \dots, M_{16}(t, f)\}) \quad (6)$$

with each $M_k(t, f)$ corresponding to the DNN prediction for channel k , as described in section II-D. The whitened spatial covariance $\mathbf{P}(t, f)$ corresponds to:

$$\mathbf{P}(t, f) = \begin{bmatrix} \phi_{1,1}(t, f) & \dots & \phi_{1,K}(t, f) \\ \vdots & \ddots & \vdots \\ \phi_{K,1}(t, f) & \dots & \phi_{K,K}(t, f) \end{bmatrix} \cdot \quad (7)$$

$$= \hat{\Phi}_{BB}(t, f)^{-1}\hat{\Phi}_{XX}(t, f)$$

The direction of arrival $\theta_t^* \in \mathcal{D} = \{v \in \mathbb{R}^3 : \|v\|_2 = 1\}$ can be estimated for each time frame as the potential direction that maximizes the beamformer power:

$$\theta_t^* = \arg \max_{\theta} (E(\mathbf{P}(t, f), \theta)), \quad (8)$$

and the power corresponds to:

$$E(\mathbf{P}(t, f), \theta) = \sum_{u=0}^K \sum_{v=0}^K \sum_{f=0}^F W_{u,v}(f, \theta) \phi_{u,v}(t, f), \quad (9)$$

$$W_{u,v}(f, \theta) = \exp \left(j \frac{2\pi f}{N} \left[\frac{fs}{c} (\mathbf{r}_u - \mathbf{r}_v) \cdot \theta \right] \right), \quad (10)$$

where $fs \in \mathbb{N}$ is the sample rate (samples/sec), $c \in \mathbb{R}^+$ is the speed of sound (343 m/s), $\theta \in \mathcal{D}$ is the DoA in cartesian coordinate and $\mathbf{r}_k \in \mathbb{R}^3$ is the microphone position in cartesian coordinate.

As mentioned previously, the free-field and far-field assumptions no longer hold when using all 16 microphones. To preserve the far-field assumption, only the sub array A and B are used. This configuration provides a good balance between computational complexity and localization performance, while satisfying one of the two fundamental assumptions of the conventional SRP-PHAT method.

F. Face Detection and Inverse Kinematic

Once the direction of arrival is estimated by the SSL module, the robotic arm rotates toward the target direction. During this motion, the arm transitions into the face detection configuration, as illustrated in Fig. 2. The sixth joint is tilted at 80° , which provides a wide vertical field of view (FOV) that enables the camera to detect individuals of varying heights.

MediaPipe [20] and the RGB camera are used to locate the face of the target within the image frame. When combined with the depth sensor, a simple pinhole camera model [21] and 3D geometric reconstruction are employed to estimate the (x, y, z) coordinate of the center of the face relative to the manipulator's reference axis. The RGB camera captures a single frame, while the depth sensor acquires multiple frames that are subsequently averaged to improve robustness.

The IK module requires the desired position and orientation of the end-effector, along with an initial angular guess for each joint. The target end-effector position is provided by the output of the face-detection module, while its orientation is computed based on the current system state. Initial joint angle guesses are obtained by measuring the joint angles when the arm is in the desired configuration; this initialization also biases the IK solver towards the desired solution. Once a valid solution is found, the manipulator is reconfigured to the optimized pose. Fig. 1a illustrates the arm configuration when tracking a target at 45° .

G. Speech enhancement

Once the arm reaches its optimized configuration, the MVDR can beamformer is applied to suppress noise and produce a cleaner signal. The MVDR method minimizes the

output signal variance while enforcing a unit gain constraint on a reference microphone, thereby preventing signal distortion. The corresponding filter weights are computed using the following equation [22]:

$$\mathbf{w}_{mvdr}(f) = \frac{\Phi_{BB}^{-1}(f)\Phi_{XX}(f)}{\text{Tr}(\Phi_{BB}(f)^{-1}\Phi_{XX}(f))}\mathbf{u}, \quad (11)$$

where $\text{Tr}(\cdot)$ denotes the trace operator and $\mathbf{u} \in \{0, 1\}^K$ is a one-hot vector used to select the reference channel. The target and speech SCMs, Φ_{XX} and Φ_{BB} , are computed using the predicted mask $M_k(t, f)$ for each channel k :

$$\hat{X}_k(t, f) = Y_k(t, f)M_k(t, f), \quad (12)$$

$$\hat{B}_k(t, f) = Y_k(t, f)(1 - M_k(t, f)), \quad (13)$$

$$\hat{\mathbf{X}}(t, f) = [\hat{X}_1(t, f) \quad \dots \quad \hat{X}_K(t, f)]^T \quad (14)$$

$$\hat{\mathbf{B}}(t, f) = [\hat{B}_1(t, f) \quad \dots \quad \hat{B}_K(t, f)]^T \quad (15)$$

$$\Phi_{XX}(f) = \sum_{t=0}^T \hat{\mathbf{X}}(t, f)\hat{\mathbf{X}}(t, f)^H, \quad (16)$$

$$\Phi_{BB}(f) = \sum_{t=0}^T \hat{\mathbf{B}}(t, f)\hat{\mathbf{B}}(t, f)^H. \quad (17)$$

For SE, each mask is used individually (as opposed to SSL where they are pooled in a single mask) to provide better enhancement performance.

It is important to note that, for this enhancement approach, the reference channel is always the 16th. In most frameworks, the reference channel can be selected arbitrarily since no obstacle blocks the propagation path between the microphones and the array aperture is limited. Hence, the signals received at each microphone are similar. In the proposed system, however, the aperture can reach up to 1 m and the fourth sub-array is positioned close to the mouth of the target. This placement enables the capture of a higher-quality speech reference and provides more reliable information to the MVDR beamformer. For SE, the complete SCM is calculated non-recursively because speech recognition can be performed offline, while for SSL the localization is estimated on a frame-by-frame basis, which requires the use of an online SCM.

III. EXPERIMENTS AND RESULTS

The section is organized as follows. First, the SSL performance is evaluated, as it constitutes a key component of the proposed pipeline. Second, the system is compared against traditional static microphone arrays to demonstrate its performance advantages. Finally, the complete enhancement pipeline, from SSL to speech-to-text, is validated to demonstrate the overall feasibility of the proposed approach. In all subsequent experiments, a printed image of a human face was mounted on a Genelec 8020D loudspeaker to mimic a human speaker.

A. Sound Source localization

To validate the SSL performance of the system, a three-second speech segment is recorded at 18 different DoAs ($0^\circ, 20^\circ, 40^\circ, \dots, 340^\circ$). In addition, six different noise types (vacuum pump, drill, engine, electric noise, compressed air, mine noise) are recorded at 18 different DoAs ($10^\circ, 30^\circ, 50^\circ, \dots, 350^\circ$). Each speech recording is mixed with each noise recording at four different SNR levels ($-5, 0, 5, 10$) dB for a total of 1,944 mixtures per SNR level. Since SSL is the first stage of the pipeline, the arm configuration would theoretically be random; therefore, only one arm configuration is evaluated. The tested configuration is shown in Fig. 1b. For evaluation, the selected output is the median azimuth θ_t^* computed over all time frames t . The adaptation rate α is set to 0.1.

The SSL performance are evaluated using the error rate with a $\pm 15^\circ$ tolerance (ER_{15}). The camera has a horizontal field of view of approximately 40° . Empirical evaluation shows that, with a 15° localization error, the system can still reliably locate faces when the manipulator is correctly oriented. Table I shows the ER_{15} , which demonstrates that the performance remains acceptable even at low SNR levels. As expected, the oracle mask outperforms the DNN-based mask. However, as the input SNR increases, the success rate improves, and the performance of the DNN IRM progressively approaches that of the oracle IRM.

TABLE I: ER_{15} with oracle IRM and DNN IRM

SNR (dB)	Oracle ER_{15} (%)	DNN ER_{15} (%)
-5	89.45	79.89
0	93.78	90.43
5	96.81	95.42
10	98.41	98.20

B. Speech Enhancement

The enhancement performance is compared against four different static microphone arrays and a small shotgun microphone. Figure 1 shows all audio capture devices. The first three static arrays correspond to the microphones mounted on the robotic arm in a fixed configuration. The fourth static array is the one used in [23], and demonstrates the performance of a more conventional array, not directly mounted on the robot joints. Finally, a small shotgun microphone is mounted near the end-effector of the arm. Enhancement performance are evaluated using two metrics: 1) the Scale-Invariant Signal-to-Distortion Ratio (SI-SDR) [24]; and 2) the word error rate (WER). Speech recognition is performed using the base Whisper model [25]. Both metrics are computed using oracle and DNN-based IRM. For each recording device, speech is recorded from four different DoAs ($45^\circ, 135^\circ, 225^\circ, 315^\circ$), while noise is recorded from 18 DoAs ($10^\circ, 30^\circ, 50^\circ, \dots, 350^\circ$). It should be noted that, for recordings made with the optimized array and the shotgun microphone, the arm is reconfigured as a function of the speech DoA, so the end-effector faces the speaker. Four different speech segments and six different noise types

(vacuum pump, drill, engine, electric noise, compressed air, mine noise) are recorded. Each speech segment from the four DoAs is mixed with each noise segment from all noise DoAs at four SNR levels ($-5, 0, 5, 10$) dB, resulting in a total of 10,368 mixes per SNR level.

To ensure a fair comparison between the audio capture devices, a reference gain is computed using the first four microphones of the optimized array. This gain is used to normalize the noise such that the input SNR equals to ($-5, 0, 5, 10$) dB. For a given test configuration (e.g. speech from 45° and drill noise from 70°), the same noise gain is applied across all recording devices. This approach makes it possible to account for geometric differences between the devices and for the way sound is captured by the various microphone arrays.

TABLE II: SI-SDR at various SNR levels (dB)

M.	SNR	Optim.	Stat. 1	Stat. 2	Stat. 3	Stat. 4	Shot.
Oracle	-5	19.31	16.58	16.65	16.93	17.12	-
	0	23.22	20.41	20.47	20.89	21.08	-
	5	27.07	24.13	24.24	24.81	24.96	-
	10	30.90	27.86	28.02	28.78	28.86	-
DNN	-5	18.51	15.56	15.56	16.05	16.32	0.11
	0	22.95	20.44	20.31	20.71	20.94	3.67
	5	27.09	24.78	24.68	25.09	25.25	7.72
	10	31.00	28.81	28.83	29.36	29.43	12.13

TABLE III: WER (%) at various SNR levels (dB)

M.	SNR	Optim.	Stat. 1	Stat. 2	Stat. 3	Stat. 4	Shot.
Oracle	-5	10.01	22.70	22.17	24.46	19.77	-
	0	8.32	16.53	15.69	17.68	13.16	-
	5	7.84	13.66	12.81	14.57	11.23	-
	10	7.62	12.73	11.87	13.35	10.68	-
DNN	-5	17.34	36.79	34.68	39.11	36.13	40.35
	0	10.46	22.78	21.98	24.78	19.20	25.24
	5	8.04	15.60	15.00	16.74	12.44	16.21
	10	7.35	11.99	11.59	12.99	10.50	11.39

The SI-SDR is computed as a weighted average, with each segment weighted proportionally to its duration. A similar procedure is used for the WER, except that each segment is weighted according to its number of words. In addition, the WER are clipped to 100%, since in some cases, mostly at low SNR levels, the speech-to-text module produced more words than there are in the reference speech, resulting in WER values exceeding 100%. Overall, the results show that the optimized array outperforms the other configurations by a substantial margin. In contrast, the static arrays and shotgun microphone exhibit to perform similarly across the different test conditions. These findings suggest that mounting the microphones directly on the arm without any optimization strategy yields performance comparable to that of a conventional static array.

To further validate that the optimized array provides the best performance, the same experiment is repeated, except that the MVDR filter weights are computed using each channel in turn as the reference. For each configuration, the minimum WER obtained across all possible reference

channels is selected, and shown in Table IV. Results indicate that even if the reference yielding the best WER could be selected *a priori*, the optimized array would still outperform the static arrays. The results also show that selecting the 16th microphone as the reference channel for the optimized array is a reasonable design choice: it surpasses the best-case performance of all static arrays, although it does not strictly maximize performance for the optimized array itself.

TABLE IV: Minimum WER in % at various SNR levels (dB)

Mask	SNR	Optim.	Stat. 1	Stat. 2	Stat. 3	Stat. 4
Oracle	-5	7.06	14.70	13.59	13.99	11.81
	0	5.69	9.85	9.11	9.27	7.64
	5	5.34	7.89	7.49	7.68	6.27
	10	5.23	7.29	6.95	7.15	5.83
DNN	-5	13.16	25.58	23.37	25.53	24.40
	0	7.47	14.74	12.97	13.74	11.83
	5	5.62	9.33	8.25	8.76	7.04
	10	5.16	7.03	6.40	6.88	5.74

C. Overall system

The following experiment validates the complete pipeline, from the SSL module to speech-to-text recognition. A five-second speech segment is played from a loudspeaker, while, simultaneously, a second loudspeaker emits noise. During this period, the system records the signals and performs SSL. Once the azimuth angle is estimated, the robot rotates to face the target. The face detection and IK modules then estimate the face coordinates and move the end-effector close to the target. Finally, one loudspeaker plays speech, and another plays noise, and both signals are recorded independently for subsequent evaluation.

The complete system is evaluated using six different speech-noise DoA configurations, listed in Table V. The same four different speech segments and six noise types are used as in the previous experiments. These six configurations are also tested in real-world conditions at approximately the same four SNR levels ($-5, 0, 5, 10$) dB. Figure 4 illustrates the SI-SDR improvement as a function of the input Si-SDR. During testing, the localization onlys once (red dot). Figure 5 presents the WER improvement relative to the unenhanced baseline. The results show that speech enhancement has a substantial impact on the WER at low input SI-SDR levels. However, the figure also indicates that, in some cases, the MVDR processing negatively affects the transcription output. Finally, across all tested scenarios, the face detection and IK modules operate flawlessly.

TABLE V: Different speaker configuration during testing

Case	1	2	3	4	5	6
Speech DoA	30°	60°	90°	120°	140°	170°
Noise DoA	270°	240°	340°	270°	20°	300°

IV. CONCLUSION

This paper presents an efficient method for optimizing the position of a microphone array mounted on a robotic

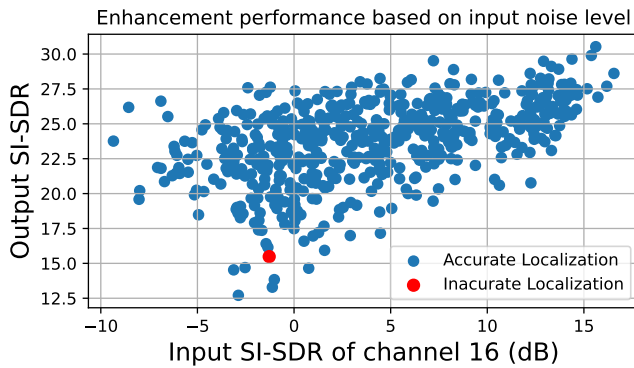


Fig. 4: Output SI-SDR vs input SI-SNR at channel 16

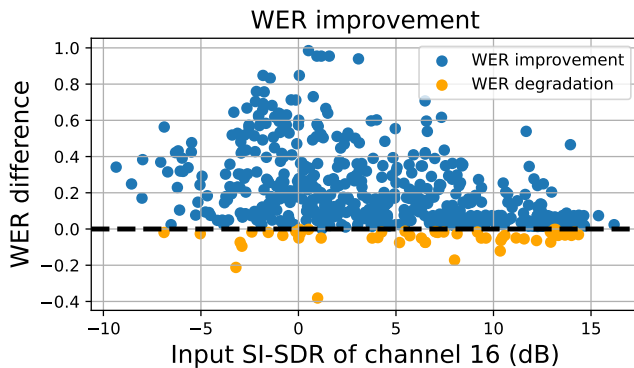


Fig. 5: WER improvement vs the input SNR at channel 16

arm to improve speech enhancement and ASR in a noisy environments. The method relies on four main modules: 1) SSL based on a modified version of SRP-PHAT; 2) face detection using MediaPipe; 3) an IK module; and 4) an MVDR beamformer coupled with a DNN that estimates time-frequency masks for speech-noise separation. Experimental results demonstrate that the complete enhancement pipeline is effective, outperforming traditional recording devices, and that the proposed method is robust to ambient noise. Future work will focus on a real-time implementation with a lighter DNN architecture and smart reference channel selection to improve performance.

ACKNOWLEDGEMENT

Generative AI (ChatGPT) was used to improve text in this paper.

REFERENCES

- [1] H. G. Okuno and K. Nakadai, "Robot audition: Its rise and perspectives," in *Proc. of the IEEE ICASSP*, pp. 5610–5614, 2015.
- [2] M. Norda, C. Engel, J. Rennies, J.-E. Appell, S. C. Lange, and A. Hahn, "Evaluating the efficiency of voice control as human machine interface in production," *IEEE T-ASE*, vol. 21, no. 3, pp. 4817–4828, 2024.
- [3] M. C. Bingol and O. Aydogmus, "Performing predefined tasks using the human-robot interaction on speech recognition for an industrial robot," *Eng. Appl. Artif. Intell.*, vol. 95, p. 103903, 2020.
- [4] I. Kadri, S. A. Selouani, M. Ghribi, R. Ghali, and S. Mekhoukh, "LLM-driven agent for speech-enabled control of industrial robots: A case study in snow-crab quality inspection," *RINENG*, vol. 27, p. 106660, 2025.

- [5] H. Erdogan, J. R. Hershey, S. Watanabe, M. I. Mandel, and J. L. Roux, "Improved MVDR beamforming using single-channel mask prediction networks," in *Proc. of Interspeech*, pp. 1981–1985, 2016.
- [6] J. Heymann, L. Drude, and R. Haeb-Umbach, "Neural network based spectral mask estimation for acoustic beamforming," in *Proc. of the IEEE ICASSP*, pp. 196–200, 2016.
- [7] X. Xiao, S. Watanabe, H. Erdogan, L. Lu, J. Hershey, M. L. Seltzer, G. Chen, Y. Zhang, M. Mandel, and D. Yu, "Deep beamforming networks for multi-channel speech recognition," in *Proc. of the IEEE ICASSP*, pp. 5745–5749, 2016.
- [8] B. Li, T. N. Sainath, R. J. Weiss, K. W. Wilson, and M. Bacchiani, "Neural network adaptive beamforming for robust multichannel speech recognition," in *Proc. of Interspeech*, pp. 1976–1980, 2016.
- [9] A. Pandey, B. Xu, A. Kumar, J. Donley, P. Calamia, and D. Wang, "TPARN: Triple-path attentive recurrent network for time-domain multichannel speech enhancement," in *Proc. of the IEEE ICASSP*, pp. 6497–6501, 2022.
- [10] T. Ochiai, S. Watanabe, T. Hori, J. R. Hershey, and X. Xiao, "Unified architecture for multichannel end-to-end speech recognition with neural beamforming," *IEEE JSTSP*, vol. 11, no. 8, pp. 1274–1288, 2017.
- [11] F. Grondin and F. Michaud, "Lightweight and optimized sound source localization and tracking methods for open and closed microphone array configurations," *Robot. Auton. Syst.*, vol. 113, pp. 63–80, 2019.
- [12] M.-A. Maheux, C. Caya, D. Létourneau, and F. Michaud, "T-Top, a SAR experimental platform," in *Proc. of the ACM/IEEE HRI*, pp. 904–908, 2022.
- [13] J. Yu and K. D. Donohue, "Geometry descriptors of irregular microphone arrays related to beamforming performance," *EURASIP J. Adv. Signal Process.*, no. 1, p. 249, 2012.
- [14] V. Tourbabin and B. Rafaely, "Theoretical framework for the optimization of microphone array configuration for humanoid robot audition," *IEEE/ACM Trans. Audio Speech Lang. Process.*, vol. 22, no. 12, pp. 1803–1814, 2014.
- [15] R. Moisseev, G. Itzhak, and I. Cohen, "Array geometry optimization for region-of-interest near-field beamforming," in *Proc. of the IEEE ICASSP*, pp. 576–580, 2024.
- [16] Y. Zhang, Z. Li, and K. F. C. Yiu, "Optimal microphone array placement design using the bayesian optimization method," *Sensors*, vol. 24, no. 8, p. 2434, 2024.
- [17] F. Grondin, J.-S. Lauzon, J. Vincent, and F. Michaud, "GEV beamforming supported by DOA-based masks generated on pairs of microphones," in *Proc. of Interspeech*, pp. 3341–3345, 2020.
- [18] C. K. A. Reddy, V. Gopal, R. Cutler, E. Beyrami, R. Cheng, H. Dubey, S. Matushevych, R. Aichner, A. Aazami, S. Braun, P. Rana, S. Srinivasan, and J. Gehrke, "The INTERSPEECH 2020 deep noise suppression challenge: Datasets, subjective testing framework, and challenge results," in *Proc. of Interspeech*, pp. 2492–2496, 2020.
- [19] T. Ko, V. Peddinti, D. Povey, M. L. Seltzer, and S. Khudanpur, "A study on data augmentation of reverberant speech for robust speech recognition," in *Proc. of the IEEE ICASSP*, pp. 5220–5224, 2017.
- [20] C. Lugaresi, J. Tang, H. Nash, C. McClanahan, E. Uboweja, M. Hays, F. Zhang, C.-L. Chang, M. G. Yong, J. Lee, W.-T. Chang, W. Hua, M. Georg, and M. Grundmann, "MediaPipe: A framework for building perception pipelines," *arXiv preprint arXiv:1906.08172*, 2019.
- [21] K. Khoshelham and S. O. Elberink, "Accuracy and resolution of kinect depth data for indoor mapping applications," *Sensors (Basel, Switzerland)*, vol. 12, no. 2, pp. 1437–1454, 2012.
- [22] M. Souden, J. Benesty, and S. Affes, "On optimal frequency-domain multichannel linear filtering for noise reduction," *IEEE/ACM Trans. Audio Speech Lang. Process.*, vol. 18, no. 2, pp. 260–276, 2010.
- [23] P.-O. Lagacé, F. Ferland, and F. Grondin, "Ego-noise reduction of a mobile robot using noise spatial covariance matrix learning and minimum variance distortionless response," in *Proc. of the IEEE/RSJ IROS*, pp. 3533–3538, 2023.
- [24] J. L. Roux, S. Wisdom, H. Erdogan, and J. R. Hershey, "SDR – half-baked or well done?," in *Proc. of the IEEE ICASSP*, pp. 626–630, 2019.
- [25] A. Radford, J. W. Kim, T. Xu, G. Brockman, C. McLeavey, and I. Sutskever, "Robust speech recognition via large-scale weak supervision," *arXiv preprint arXiv:2212.04356*, 2022.